From Colloidal Aggregates to Layered Nanosized Structures in Polymer−Surfactant Systems. 1. Basic Phenomena

Epameinondas Leontidis,*,† Tasoula Kyprianidou-Leodidou,† Walter Caseri,‡ Pierre Robyr,‡ Frank Krumeich,§ and Kyriacos C. Kyriacou||

Department of Chemistry, University of Cyprus, P.O. Box 20537, 1678 Nicosia, Cyprus, Institut für Polymere, ETH Zentrum, CH-8092 Zürich, Switzerland, Laboratorium für Anorganische Chemie, ETH Zentrum, CH-8092 Zürich, Switzerland, and The Cyprus Institute of Neurology and Genetics, P.O. Box 3462, 1683 Nicosia, Cyprus

Received: August 21, 2000; In Final Form: November 12, 2000

In this work, we examine the rich crystallization behavior that occurs in Pb^{II}/S^{-II}/poly(ethylene oxide) (PEO)/sodium dodecyl sulfate (SDS) systems, in which the anionic surfactant interacts strongly with the polymer molecules, forming micellar aggregates attached to the polymer chains above the critical association concentration. Lead sulfide crystallites are *formed in the vicinity of* polymer-bound micelles by adding lead and sulfide ions to the polymer−surfactant solution. Surfactant-stabilized inorganic particles adsorbed on the polymer chains combine through a polymer-mediated bridging flocculation mechanism to produce characteristic rodlike colloidal aggregates. Under certain conditions, these evolve into a range of metastable structures, composed of lead sulfide, PbS, and lead dodecyl sulfate, $Pb(DS)_2$. XRD analysis of the metastable reaction products allows us to follow the slow kinetics of their formation and reveals a well-defined layered structure, based on lead dodecyl sulfate, the thickness of which is determined by the length of the surfactant chains. Elemental analysis, ^{13}C- and ^{207}Pb−NMR spectroscopy, FTIR spectroscopy, XPS, and HRTEM are used to characterize these superstructures. At other pH values and system compositions, the production of pure PbS or pure $Pb(DS)_2$ is favored, by appropriate tuning of the concentrations of Pb^{2+} and S^{2-} ions. The resulting unexpectedly rich crystallization behavior illustrates the complexity of colloidal aggregation phenomena in polymer−surfactant solutions and the significance of coupling colloidal aggregation to ionic equilibria.

I. Introduction

This study deals with aqueous solutions containing polymer−surfactant aggregates as media for inorganic crystallization. The use of supramolecular systems for the control of inorganic crystallization has become an area of intense research activity in the past decade.[1] The goal is to control the size, shape, morphology, and polydispersity of the crystals but also to produce novel organic/inorganic nanocomposite materials with tunable magnetic,[2] electrical,[3] optical,[4] and catalytic[5] properties.

Some years ago, we examined the size and shape variation of PbS nanocrystals formed in polymer−surfactant solutions.[6] The production of nanocrystalline PbS has been extensively studied in recent years, because PbS is a prominent semiconductor. Nanoparticles of PbS have been synthesized in reversed micelles,[7] in lyotropic surfactant phases,[8] under Langmuir monolayers at the air−water interface,[9] with topotactic reactions in Langmuir−Blodgett films[10] and lead alkanoate multilayers,[11] in polymer films, gels, and block copolymers,[12] and also in aqueous or organic solutions with proper stabilizing agents.[13] Recent work has shown that the shape and overall morphology of PbS nanocrystals can indeed be controlled by templating phenomena in a variety of systems, usually involving a strong interaction of Pb^{2+} ions and a moiety of the template.[12,14] The use of relatively low polymer and surfactant concentrations but a high Pb^{2+} concentration results in coprecipitation of PbS crystals and polymer in the form of a gel.[6] Upon variation of the composition of the crystallizing system, taking into account the known physicochemical characteristics of polymer−surfactant solutions,[16] we unexpectedly obtained an organic/inorganic nanocomposite material in the form of long rodlike particles, which evolved into a layered structure with time.[15] The present study is an attempt for a complete understanding of the crystallization phenomena occurring in these complex systems, at the limit of low surfactant and polymer concentrations.

Water-soluble nonionic polymers, such as poly(ethylene oxide) (PEO) or poly(vinyl pyrrolidone) (PVP), interact strongly with anionic surfactants in aqueous solutions.[16,17] The surfactants associate with the polymer chains forming micellar aggregates at a critical association concentration (cac), which is often considerably lower than the critical micellar concentration (cmc) of the surfactant in pure water. The micelles formed in the system PEO−sodium dodecyl sulfate (SDS) have been particularly well characterized in the last 30 years[16,17] and have become a standard reference system. We decided to use PEO−SDS solutions as crystallization media for PbS on the basis of the following considerations:

(a) Counterions are strongly adsorbed on micellar surfaces of the opposite charge; hence, crystallization occurs at a much faster rate at the surface of the micelles than in the bulk of the solution. If the surface of SDS micelles is saturated with Pb^{2+}, heterogeneous nucleation should be the main, if not the only, PbS crystal formation process in such a system.

* To whom correspondence should be addressed.
† University of Cyprus.
‡ Institut für Polymere.
§ Laboratorium für Anorganische Chemie.
|| The Cyprus Institute of Neurology and Genetics.

10.1021/jp0029966 CCC: $20.00
Published on Web 04/17/2001

(b) Pb^{2+} is known to precipitate the surfactant (SDS); hence, it may be possible to influence the crystallization conditions toward various possible products, by tuning pH and solution composition.

(c) The polymer can act as a stabilizer for the crystal dispersion, preventing the direct precipitation of the product. On the other hand, the polymer can help to connect the crystals into loose flocs, through a bridging flocculation mechanism.[18]

Some of the above points were verified in a preliminary investigation.[15] However, with the resulting picture of the crystallization phenomena being very complex, a thorough investigation of the system was considered necessary. This is the subject of the present paper.

The outline of the paper is as follows: Section II gives details about all of the experimental methods used. The results and discussion section, section III, is divided into six subsections. These describe the basic crystallization experiment, provide a working hypothesis for the kinetic mechanisms and the thermodynamic driving forces in the crystallization process, present our experimental investigations of the structure of the typical composite product formed from crystallization, examine the fundamental role of the pH value, detail the influence of surfactant and polymer concentrations and solution composition on the crystallization process, and explain the different results obtained when lead is introduced as the nitrate or as the acetate salt. In section IV, we summarize by recalling the most important insights gained by the present investigation and listing the significant questions that still remain unanswered.

II. Experimental Methods

Materials. PEO was from Polysciences Inc., with nominal molecular weights of 2×10^5 and 5×10^6 Dalton, and was used as received. SDS (99% purity) was obtained from Sigma or Fluka and used without further purification. It contains some surface-active impurities (mostly dodecanol), as evidenced from a maximum in the surface tension vs concentration plot; however, we did not consider purification necessary, because we are not dealing here with a delicate surface chemistry experiment. $Na_2S \cdot 9H_2O$ was purchased from Sigma and used as received. Because it is highly hygroscopic, the concentrations of sulfide solutions obtained from this material were determined gravimetrically, by precipitation of PbS from a $Pb(NO_3)_2$ solution. All other chemicals used in this work were used as received. ^{13}C-labeled sodium acetate and acetic acid (label at the carboxyl group, 99% isotopic purity) were obtained from Cambridge Isotope Laboratories.

Procedures for Carrying out Crystallization Experiments. In a typical experiment, the ratios of the two components in the PEO/SDS system were selected in a way that the system contained mostly polymer-bound micelles (no free micelles). The SDS concentration must thus be between the cac and the cmc. These two concentrations are well-known for the PEO/SDS system[16,17] (*the cac is approximately 4 mmol/l*) but were also confirmed with conductivity measurements. SDS concentrations between 4 and 8 mmol/L have been employed in most experiments reported here. PEO of molecular weights of 2×10^5 and 5×10^6 and polymer concentrations between 3 and 15 g/L were employed. At this concentration range, the solution is semidilute for the polymer with the higher molecular weight and dilute to semidilute for the lower-molecular-weight polymer.[19] To these solutions were added Pb^{2+} salts (lead acetate or lead nitrate, to a final total Pb^{II} concentration of 3−4 mmol/L) and subsequently S^{2-} ions (sodium sulfide, to a final total S^{-II} concentration of 3−4 mmol/L). The pH value of the solutions was adjusted with concentrated nitric or acetic acid (for acidic solutions) and with sodium hydroxide or sodium acetate for basic solutions. After the initial addition of lead ions, the PEO/SDS solution became cloudy, because of the association of Pb^{2+} with SDS. Upon addition of S^{2-}, the solution acquired immediately a brown-black color. The colloidal particles formed remained in suspension at room temperature (20−25 °C) without stirring, being stabilized by the surfactant and by the polymer chains. Direct dipping of Formvar-covered copper grids provided samples for transmission electron microscopy work. Small amounts of the reaction solution were periodically withdrawn and analyzed by UV spectroscopy. Powder samples for XRD, elemental analysis, solid state NMR spectroscopy, FTIR spectroscopy, etc. were obtained mostly by vacuum filtration of the colloidal solutions using filters with pore diameters of 0.2 or 0.5 μm and, in some cases, by prolonged centrifugation. The solids were always washed with large amounts of water and dried at atmospheric pressure and room temperature for at least 24 h.

Lead dodecyl sulfate, $Pb(DS)_2$, was synthesized for reference purposes by the reaction between 0.1 M lead nitrate and 0.2 M SDS solutions at ambient temperature. The compound, which is quite insoluble in water (see section III.2), precipitated easily at room temperature with almost 100% yield. The precipitate was filtered and washed with sufficient cold water to remove excess lead and dodecyl sulfate ions (the presence of the latter can be avoided if a slight excess of lead ions is used in the reaction). The precipitate was dried at room temperature under 100 mbar vacuum for 24 h. Elemental analysis of the resulting white sheetlike solid yielded C, 39.2%; H, 6.43%; S, 8.65% (theoretical values are C, 39.1%; H, 6.78%; S, 8.68%). Apparently no water molecules cocrystallize with $Pb(DS)_2$ under the conditions used.

Lead acetate-dodecyl sulfate, Pb(Ac)(DS), was synthesized in a similar way as $Pb(DS)_2$, by the reaction of 0.2 M lead acetate and 0.1 M SDS solutions at ambient temperature. It was handled and dried exactly as $Pb(DS)_2$. Elemental analysis of the white sheetlike precipitate yielded C, 31.5%; H, 5.32%; S, 5.70% (theoretical values are C, 31.6%; H, 5.27%; S, 6.03%).

Spectroscopic Investigation. UV spectra of the reaction solutions were obtained with a Shimadzu 160A UV−vis spectrophotometer. FTIR spectra of the solid products were obtained with a Shimadzu FTIR-8501 spectrometer using the KBr-pellet method. ^{207}Pb NMR and ^{13}C NMR spectra were run on a Chemagnetics Infinity 300 MHz spectrometer, using a double-tuned 4 mm Chemagnetics MAS probe head. The ^{13}C spectra were measured with cross-polarization ($^1H \rightarrow {}^{13}C$), under MAS conditions, with TPPM ^1H decoupling.[20] The Rf amplitudes used on both channels were 70 kHz, and the cross-polarization time was 3 μs. Tetramethylsilane (TMS) was used as a reference for ^1H- and ^{13}C NMR spectra. ^{207}Pb spectra were obtained with the Hahn echo technique (echo time 50 μs). The R_f amplitude for ^{207}Pb was 100 kHz. Continuous-wave ^1H decoupling with R_f amplitude of 50 kHz was used. PbS was used as reference for the ppm scale ($w_0 = 62.8614$ MHz). The composite material for the ^{13}C NMR investigation was prepared using a solution of carboxyl-labeled lead acetate, produced from labeled acetic acid through its stoichiometric neutralization reaction with PbO in aqueous solution.

X-ray Measurements. X-ray powder diffraction spectra were obtained using a Siemens D5400 diffractometer at room temperature with Cu Kα radiation (λ=1.54 Å).

XPS Measurements. These were performed on a Specs Sage 100 instrument, at a pressure of 10^{-9} mbar, with Mg Kα

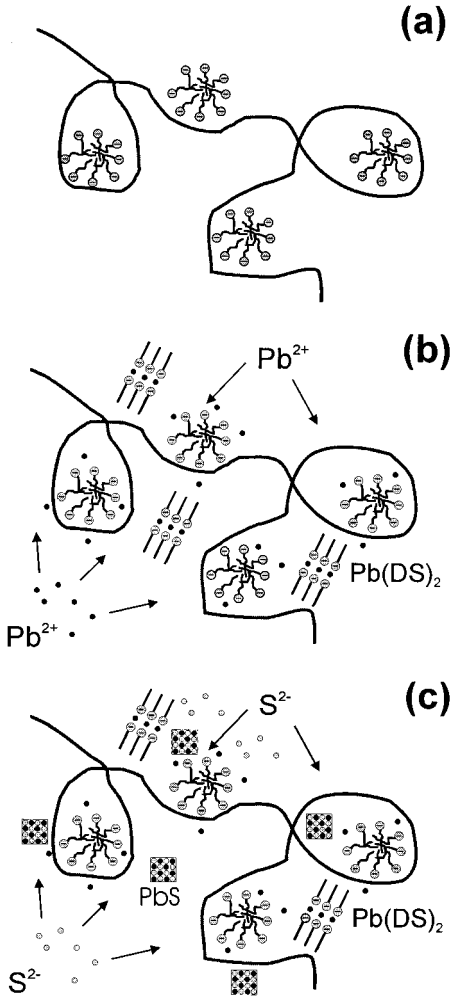

Figure 1. Schematic representation of the crystallization processes in this work. (a) SDS micelles adsorb on polymer chains. (b) Addition of Pb^{II} leads to formation of $Pb(DS)_2$, while Pb^{2+} ions concentrate around the SDS micelles. (c) The polymer-bound micelles serve as nucleating centers for fast PbS precipitation.

radiation, using a pass energy of 17.9 eV. For the final calibration of the energy scale, the main C(1s) peak was set to 285.0 eV. Exposure time for various peaks ranged from 8 to 20 min.

Electron Microscopy. Most of the electron microscopy work was performed at the Institute of Neurology and Genetics, Cyprus, on a JEOL-1010A instrument, with an acceleration voltage of 80 kV. High-resolution TEM work was performed at the ETH, Zürich, on a Philips CEM 30 HRTEM instrument with an acceleration voltage of 300 kV.

Other Measurements. Elemental analysis for C, H, N, S, and also for Pb content was performed by the microelemental analysis service of the ETH. Chemical analysis for "free" S (sulfur not contained in sulfate groups) in the solid products was performed by dissolving the powder in concentrated sulfuric acid, passing the evolving H_2S gas through a $Pb(NO_3)_2$ solution, and weighing the resulting PbS after filtering and drying. The cac and cmc of the PEO/SDS solutions were checked with electrical conductivity measurements.

III. Results and Discussion

III.1. Temporal Evolution of a Typical Precipitation Experiment at Close to Neutral pH Values. The starting point of a typical experiment is described schematically in Figure 1. Negatively charged SDS micelles are formed on PEO polymer chains at surfactant concentrations between the cac and the cmc (Figure 1a). Pb^{II} is added as the *acetate* salt, $Pb(Ac)_2$. As long as the concentration of Pb^{II} is less than that stoichiometrically required for complete precipitation of $Pb(DS)_2$, added Pb^{2+} ions (but also $Pb(Ac)^+$ ions) are concentrated near the micelles, because Pb^{2+} interacts strongly with SDS but also for micellar neutralization (double-layer effect;[21] Figure 1b). Addition of Na_2S leads to fast nucleation of PbS crystallites mainly along the contour of the polymer chains, because Pb^{2+} is found almost exclusively there (Figure 1c). It is important to retain this order of addition of reactants, because if Na_2S is added first S^{2-} and HS^- ions will be repelled from the negatively charged, polymer-bound SDS micelles and subsequent reaction with Pb^{2+} will occur mostly in the bulk of the solution.

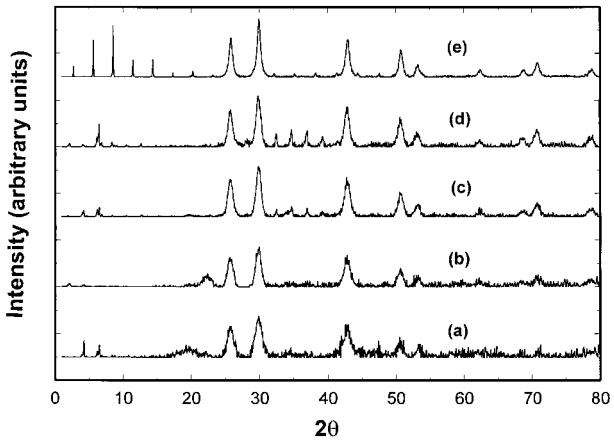

Figure 2. Time evolution of XRD *patterns* of crystallization products obtained with lead acetate at neutral pH. The *patterns* correspond to products obtained (a) 0, (b) 1, (c) 4, (d) 9, and (e) 15 days after reaction onset.

A sequence of XRD patterns and TEM pictures obtained after various reaction times show the evolution of structures in the reaction medium. The reference system, on which these observations are based, contains 3.7 mmol/L lead acetate, 3.7 mmol/L sodium sulfide, 7.8 mmol/L SDS, and 1.9 g/L PEO ($MW = 2 \times 10^5$) in a total solution volume of 80 mL, at pH values between 6.5 and 9.5, obtained by addition of concentrated acetic acid or sodium hydroxide. Figure 2 shows powder XRD patterns obtained 0, 1, 4, 9, and 15 days after the reaction was started. At short times, the characteristic peaks of lead sulfide are observed. The peaks are rather broad, indicating the formation of very small particles. Applying Scherrer's equation[22]

$$d = \frac{\alpha\lambda}{\beta \cos\theta} \tag{1}$$

where α equals 0.94 (a geometric factor), β is the half-width of the diffraction peak at the angle $2\theta = 30.12°$, and λ is the X-ray wavelength (1.54 Å), we find that the average particle diameter, d, is 100−150 Å. The XRD patterns also contain signatures of layers with three characteristic spacings at 40.5 ± 2.0 Å. The value of 40−42 Å is close to twice the fully extended length of a SDS molecule, indicating either that the core of the PbS aggregates consists of surfactant layers or that layers are forming on the outside of the PbS particles.

After approximately two weeks, one can observe the appearance of a new sequence of almost equally spaced peaks, corresponding to a lamellar structure with a spacing of 30−31 Å. Thus, XRD provides direct evidence that small PbS crystallites are formed in this system, whereas a complex phenomenon takes place at prolonged periods, which could involve

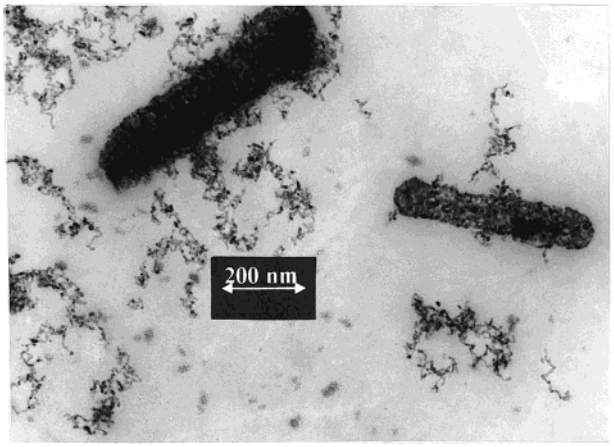

Figure 3. Particles formed during the precipitation reaction between lead acetate and sodium sulfide in the PEO/SDS system 5 days after reaction onset.

either the *dissolution* or the *organization* of PbS particles and finally leads to the formation of a layered material.

We used TEM over a time period ranging from 1 day to several weeks to observe the phenomena taking place. Figure 3 shows particles formed after 5 days in solution. An unusual aggregation phenomenon is observed: little spherical crystallites form cylindrical aggregates, 0.5−1.0 μm long, with aspect ratios between 3:1 and 6:1, depending on the pH value. The TEM picture shows also a large number of individual structures, which are believed to consist of individual polymer molecules or clusters of polymers with attached lead-containing crystals formed in the vicinity of the polymer-bound micelles. This is an indirect optical observation of polymer−surfactant association, in agreement with the prevailing ideas about this association phenomenon.[15−17] The external surface of the cylindrical aggregates themselves is composed of PbS nanocrystals, as can be observed in the high-resolution TEM picture of Figure 4a. Individual PbS crystallites with an average diameter of 100−120 Å are here clearly visible, and in some cases, even lattice fringes of the PbS structure can be observed. The size of the crystallites is in agreement with the previous estimate based on XRD patterns and Scherrer's equation. The Electron Diffraction pattern (Figure 4b) of PbS crystallites of the aggregate of Figure 4a confirms that they consist of PbS.

With increasing residence time in solution (e.g., after 2−3 weeks from reaction onset), we observe some significant changes (Figure 5). Few of the original aggregates remain in solution, whereas new longer rodlike structures appear, with lengths of several μm and aspect ratios as large as 30:1. The new structures do not consist of PbS, as evidenced by electron diffraction. These are the structures that give the lamellar signal in the XRD measurements at long reaction times. We will show below that they consist of $Pb(DS)_2$.

III.2. Kinetic Mechanisms and Thermodynamic Driving Forces. Figure 6 gives a potential kinetic mechanism for the sequence of structures described above. In accordance with this mechanism, many small nanocrystals of PbS are formed in the vicinity of the polymer chains, because lead ions are highly concentrated there, which favors the formation of PbS nuclei. The crystals do not precipitate, because their surface is saturated by surfactant molecules and they are further stabilized by the polymer. However, the crystals aggregate through a bridging flocculation mechanism mediated by the polymer chains, forming characteristic cylindrical aggregates, on which polymer chains adsorb and deliver more PbS crystallites. It is also possible that original thin sheets of $Pb(DS)_2$ form nucleation surfaces, on which PbS-loaded polymer molecules adsorb.

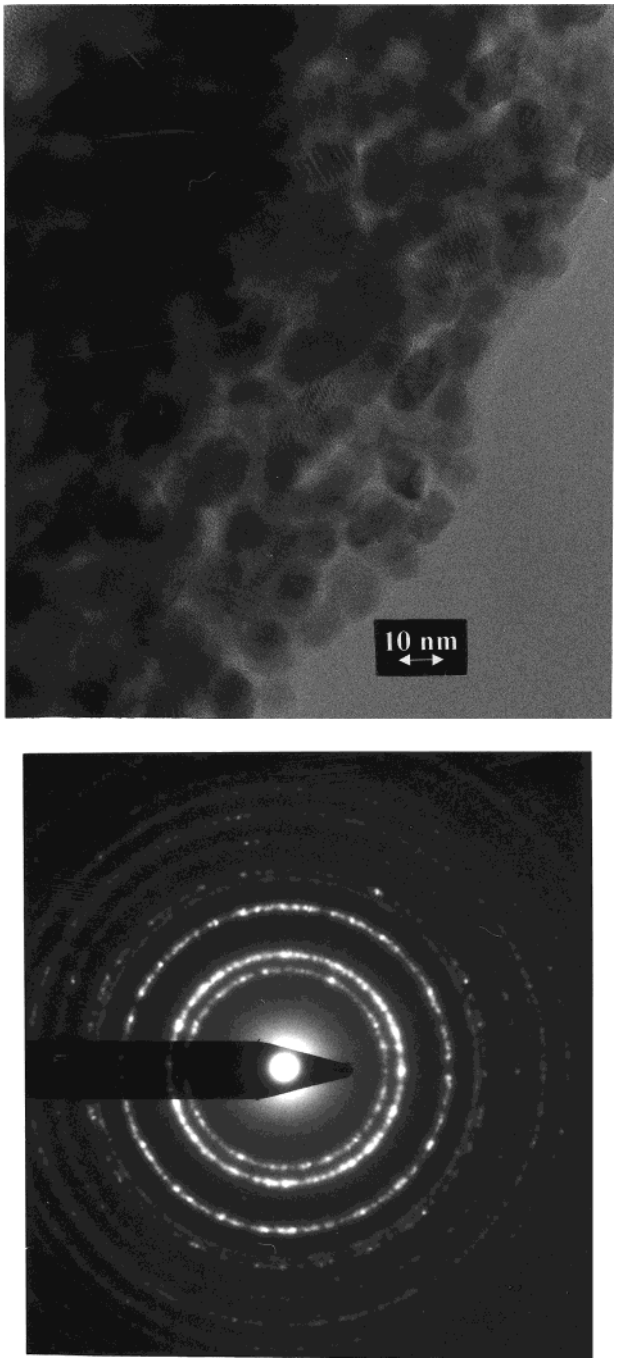

Figure 4. (a) HRTEM close-up of one of the particles of Figure 3. Individual PbS crystallites with dimensions 10−12 nm can be observed. (b) Electron diffraction pattern from a region of the aggregate of Figure 4a. Observed lattice spacings are at 3.43, 2.98, 2.10, 1.80, and 1.74 Å. Corresponding fcc-PbS (galena) spacings are at 3.429 Å [111], 2.969 Å [200], 2.099 Å [220], 1.790 Å [311], and 1.714 Å [222].

At longer times, organic superstructures start forming either *around*, from *within*, or independently from the crystal aggregates and a slow transformation takes place, with dissolution of the PbS aggregates and incorporation of lead ions into lamellae organized by the surfactant. This is not an ordinary secondary nucleation step and most probably proceeds through a variety of intermediate metastable structures, with the exact system path depending strongly on the solution composition and pH value. This last step is thus the least understood in the postulated mechanism of structure formation and evolution.

Figure 5. Evolution of structure in the crystallizing system 4 weeks after reaction onset. The initial PbS aggregates appear to dissolve, and new rodlike structures with large aspect ratios prevail.

The chemical thermodynamics of the crystallization processes in these systems is quite complex. We present the important coexisting chemical equilibria in Figure 7. First, three competing equilibria involving insoluble compounds must be considered. PbS, which is very insoluble ($K_{sp} = 8.8 \times 10^{-29}$ M^2, ref 23, but values up to 8.0×10^{-28} M^2 have been reported in the literature[24]), is already formed at low free Pb^{2+} and S^{2-} concentrations. $Pb(DS)_2$ is more soluble ($K_{sp} = 1.9 \times 10^{-10}$ M^3, ref 25), its formation being favored at acidic pH values, at which the concentration of S^{2-} is negligible and PbS formation is disfavored. Lead acetate−dodecyl sulfate, Pb(Ac)(DS), is a third insoluble product that may exist when $Pb(Ac)_2$ is used as the lead source. Pb(Ac)(DS), the K_{sp} of which does not appear to be known, is the equilibrium product formed upon precipitation of $Pb(Ac)_2$ with SDS at a high excess of acetate ions with respect to DS^- ions (e.g., 4:1 mole ratio).[26] This product is favored by high acetate concentrations with respect to DS^-, but it is not clear that it could prevail in the presence of S^{2-} ions.

In addition to the solubility equilibria, two acid−base equilibria play a prominent role in these systems. The concentration of free S^{2-} strongly depends on the pH value. The pK_a of H_2S is 7.05 and that of HS^- is 19.[23] The concentrations of S^{2-} and of HS^- decrease thus drastically between pH values of 5.5 and 8.5. For lower pH values, the formation of PbS is for this reason disfavored. The acid−base equilibrium of the acetate ion is also significantly affected by the pH (p$K_a = 4.75$)[23] when lead acetate is used as the Pb^{II} source.

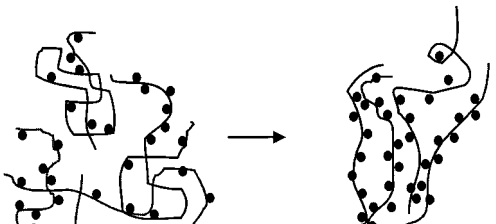

Figure 6. *Possible* bridging flocculation mechanism for the formation of rodlike PbS aggregates. The last stage of the reaction involves the production of layered organic structures. Black circles in the first three stages represent PbS nanocrystallites and in the last stage lead cations.

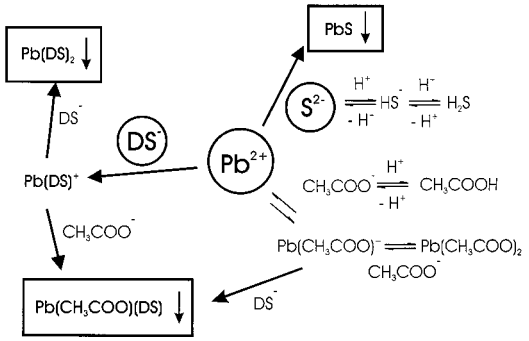

Figure 7. Schematic representation of the important chemical equilibria in the reaction system.

Finally, the lead source itself plays a role. Lead nitrate dissociates almost 100% to Pb^{2+} ions at the low concentrations used in these experiments.[27] On the contrary, $Pb(Ac)_2$ is a weak electrolyte and dissolves mostly as molecular $Pb(Ac)_2$ and $Pb(Ac)^+$.[28,29] At high pH values, Pb^{II} is complexed by hydroxide and carbonate ions.[28] In general, the degree of complexation of Pb^{2+} ions can determine the *thermodynamically predominant* precipitating species, especially at very high and very low pH values.

From the preceding discussion and Figure 7, one can conclude that the pH value, the composition of the lead source, and the relative concentrations of SDS, Pb^{II}, and S^{-II} can influence the chemical nature of the final reaction product profoundly.

III.3. Investigations of the Reaction Products at pH Values Close to Neutral. We have investigated in detail the structures obtained under the reaction conditions outlined in section III.1. At various times, we have removed small portions of the reaction medium for analysis with TEM (see results in section III.1) and UV spectroscopy. The chemical nature of the PbS aggregates

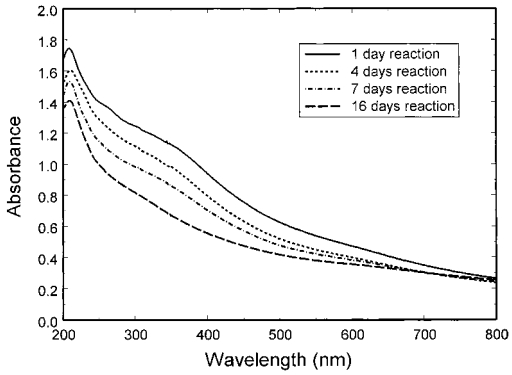

Figure 8. UV spectra of reaction solutions 1, 4, 7, and 16 days after reaction onset.

and the metastable structures formed from them at longer times was examined by filtering or centrifuging the solutions after a period of 5−15 days and analyzing the obtained powder using elemental analysis, FTIR and NMR spectroscopy, XPS, and XRD.

Atomic absorption analysis and XPS revealed that no or only a negligible amount of Na is present in the solids (<0.1%). Analysis for free sulfur, that is, S atoms other than those present in the surfactant molecules, revealed that the content of free S varies considerably between 2.0% and 3.5% of the total material mass, which is roughly 20−35% of the total S in the product. The free S content depends on the time from reaction onset in a rather uncertain way. We believe that this variability is an indication for the formation of metastable structures with changing composition involving PbS and $Pb(DS)_2$. The fact that free S is not equal to 100% of the total S already at short reaction times can be explained by the adsorption of surfactant on the PbS crystallites.

UV spectra of the reaction solution were obtained 1, 4, 7, and 16 days after reaction onset at a dilution of 8%. The results appear in Figure 8. The PbS particles are relatively large (100−150 Å, see Figure 4a), so quantum confinement effects are not clearly visible in the spectra, which have a long-wavelength tail, as expected for PbS, a weak "shoulder" at about 260 nm, and a free-Pb^{2+} peak at 210 nm. The PbS exciton peak at 600 nm and the characteristic Q-particle peak at 380−400 nm are not present here (for a detailed discussion of UV spectroscopy of Q particles of PbS, see Gallardo et al., ref 13). The most significant aspect of the spectra is that, although no precipitation of solids is visible, the absorbance of the reaction solution because of PbS but also because of Pb^{2+} ions is decreasing with time. This is an indication that structural changes are happening in the solution as the reaction proceeds.

The FTIR spectrum of the reaction product obtained at any time between 4 and 10 days from reaction onset is considerably different from the spectrum of solid $Pb(DS)_2$, resembling more those of Pb(Ac)(DS) and SDS (Figure 9). The strong dodecyl sulfate S−O stretching peaks around 1200 cm^{-1} prove that the surfactant is an integer component of the composite material obtained. The characteristic C−O−C IR frequency of the polymer (in the vicinity of 1100 cm^{-1})[30] is not visible. This band would overlap with large dodecyl sulfate bands; hence, the product might still contain small amounts of polymer. Two significant new bands are observed in the FTIR spectrum, a doublet at 1395 and 1380 and a singlet at 680 cm^{-1}. These were tentatively attributed to acetate in our previous work,[15] given their presence in the Pb(Ac)(DS) spectrum, but NMR evidence presented below proves that there is practically no acetate in the structures, whereas similar bands have been observed in

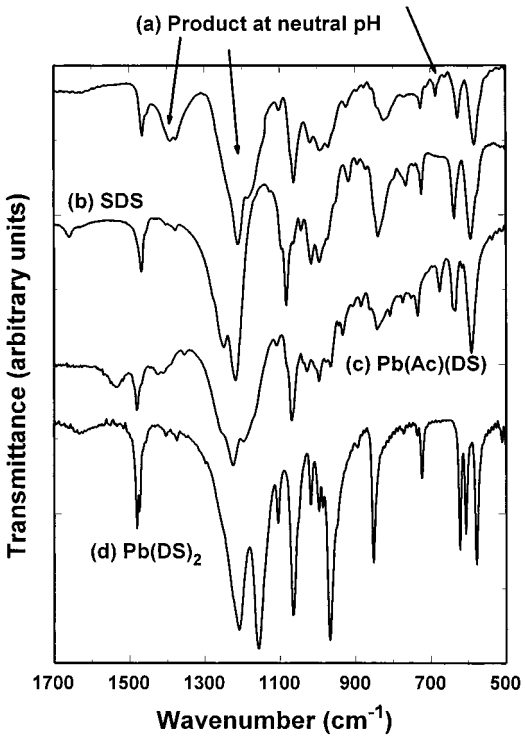

Figure 9. FTIR powder spectra (a) of the composite obtained at neutral pH, (b) of pure SDS, (c) of Pb(Ac)(DS), and (d) of pure $Pb(DS)_2$. The last two compounds are obtained by precipitation reactions between $Pb(Ac)_2$ and SDS.

systems that do not contain any acetate.[26] Besides, the acetate peak at 1530 cm^{-1}, which is clearly visible in the Pb(Ac)(DS) spectrum, is absent in the spectrum of the reaction product. Although dodecyl sulfate salts do have two weak FTIR peaks in the vicinity of 1400 cm^{-1}, usually attributed to the wagging vibration of the alpha-methylene group (with respect to the sulfate group),[31] the bands in the products discussed here are very strong. The weak but clear peak at 680 cm^{-1} is hard to assign if no acetate is present, because it is absent in SDS and $Pb(DS)_2$. The asymmetric stretch doublet of the sulfate moiety appears at 1220−1250 cm^{-1} in SDS, with the low-wavenumber peak being more intense. The same band is more symmetric in $Pb(DS)_2$ and appears at 1160−1215 cm^{-1}, whereas it appears in the reaction product and in Pb(Ac)(DS) at 1185−1215 cm^{-1}, with the low-wavenumber peak almost disappearing. The CO−S stretch peak at 855 cm^{-1} is strongly reduced in the reaction product, whereas the characteristic SO_4 deformation triplet of $Pb(DS)_2$ at 580−630 cm^{-1} appears as a doublet, practically identical to the corresponding band in SDS and in Pb(Ac)(DS). All of the evidence from the FTIR spectra indicates a different coordination of the sulfate headgroup of the surfactants in the reaction product than in SDS or $Pb(DS)_2$, with a lowering of symmetry in the composite structure. Assuming acetate is absent and given the HRTEM result in Figure 4a, one is tempted to postulate that the observed FTIR spectrum is derived by dodecyl sulfate chains adsorbed on strongly curved PbS crystallite surfaces, on which the surfactant chains are forced to adopt unusual conformations, especially in the region next to the sulfate group. It would be very useful to obtain IR-ATR spectra with polarized light[32] to further characterize the state of the surfactant chains in these products.

Several solid-state ^{207}Pb NMR spectra exist in the literature,[33] but those of $Pb(DS)_2$ or Pb(Ac)(DS) have not been measured to the best of our knowledge. In Figure 10a−d, we present solid-state ^{207}Pb NMR spectra of pure PbS, $Pb(DS)_2$, Pb(Ac)(DS),

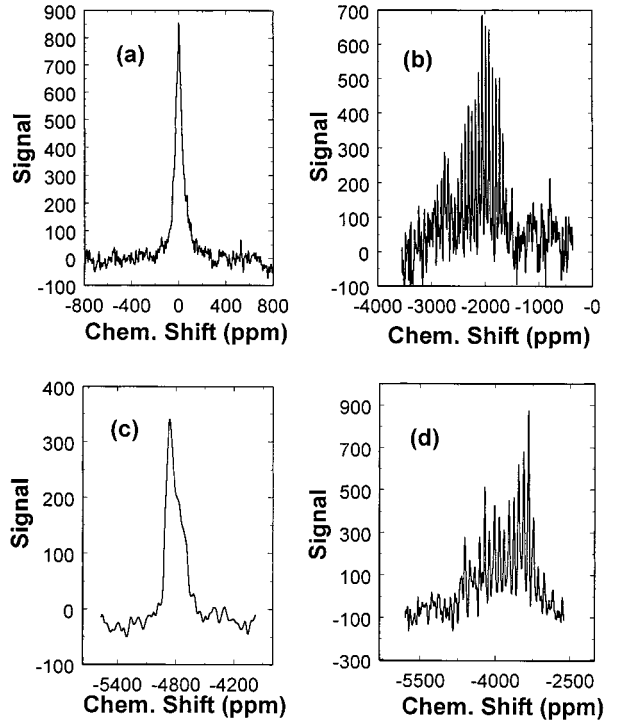

Figure 10. ^{207}Pb NMR solid-state spectra of (a) PbS, (b) $Pb(Ac)_2$, (c) $Pb(DS)_2$, and (d) Pb(Ac)(DS). The average chemical shift of PbS was set to zero.

and $Pb(Ac)_2$ for reference purposes. The PbS and $Pb(DS)_2$ spectra were acquired only statically, whereas the two other spectra were obtained under MAS conditions to reduce spectrum acquisition time. The chemical shifts of the four compounds are quite different. In Figure 11, we see the regions of the spectrum near the three observed peaks of a typical reaction product, obtained at neutral pH with lead acetate. We observe that the ^{207}Pb spectrum is extremely broad, the signals being quite dissimilar to those in the spectra of the pure lead compounds of Figure 10. The environment of lead in the reaction products is thus different, which confirms the FTIR evidence that Pb coordination is different in these metastable reaction products compared to $Pb(DS)_2$ or PbS. The very broad Pb signals (especially the peak around 0 ppm) may well be due to a "nanosize" effect, because the dimension of the primary PbS particles is 100−120 Å. ^{13}C NMR spectra (Figure 12) prove that the product contains a negligible amount of acetate, because the experiment performed with ^{13}C-labeled lead acetate provides an extremely small acetate peak, whereas the natural abundance spectrum contains no discernible acetate peak. Interestingly, this experiment indicates that the structure cannot contain any significant amount of PEO. The polymer peak should appear at 70 ppm and should overlap with the α-CH_2 peak. Integration of the triplet at 70 ppm and of the surfactant methyl peak at 14 ppm proves them to be of very nearly equal magnitude, as is implied by the surfactant stoichiometry; hence, PEO cannot contribute significantly to the peak at 70 ppm. Several peaks of different carbon atoms of the dodecyl sulfate chain are resolved in the spectra, mainly at low chemical shifts. The α-CH_2 peak (least shielded carbon atom connected to the $-OSO_3^-$ group) is here a triplet, in contrast to the singlet peak in pure $Pb(DS)_2$ (spectrum not shown here), which indicates a significantly different environment of the α-CH_2 in the two cases. We believe that the triplet arises because of different possible conformations of the surfactant headgroup area. This is in agreement with the FTIR evidence.

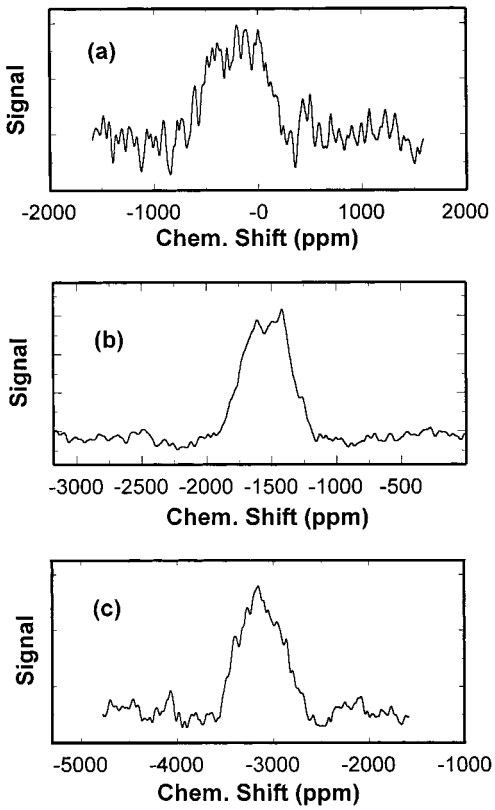

Figure 11. ^{207}Pb NMR solid-state spectrum of a product obtained at neutral pH. The three regions near the major peaks of the spectrum are shown: (a) near 0 ppm, (b) near −1500 ppm, and (c) near −3000 ppm.

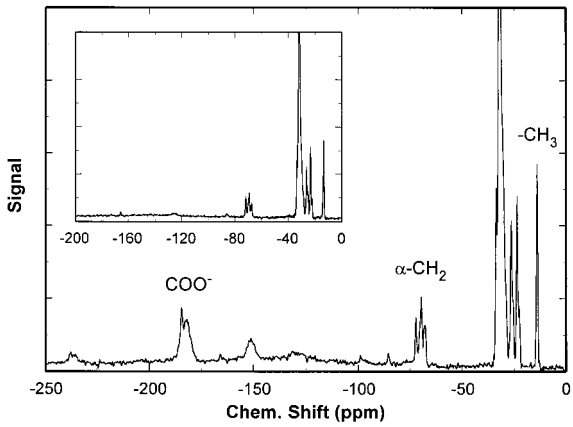

Figure 12. ^{13}C NMR solid-state spectrum of a product obtained at neutral pH. Labeled lead acetate was used in the reaction. The very small acetate peak at 70 ppm implies absence of acetate in the composite material. The inset shows a ^{13}C spectrum obtained with nonlabeled lead acetate (natural abundance spectrum).

Parts of the XPS spectrum of a product obtained 10 days after reaction onset are shown in Figure 13. The O(1s) peak at 532.3 eV is almost identical to that of SDS and is not shown here. The S(2p) spectrum (Figure 13a) shows two signals, one for the sulfate group at 168.7 eV, which is close to the corresponding line for SDS (169.0 eV), and a sulfide peak which is very broad and centered at 162 ± 1 eV. The $2p_{3/2}$ and $2p_{1/2}$ peaks of the latter cannot be resolved, making it considerably different from a reference PbS spectrum, in which the $2p_{3/2}$ and $2p_{1/2}$ signals are resolved at 160.7 and 161.7 eV. Unfortunately, the large and irregular background of the S(2p) peak does not permit unambiguous peak integration for an estimation of the sulfide-to-sulfate ratio. The complete S(2p) spectrum shows that

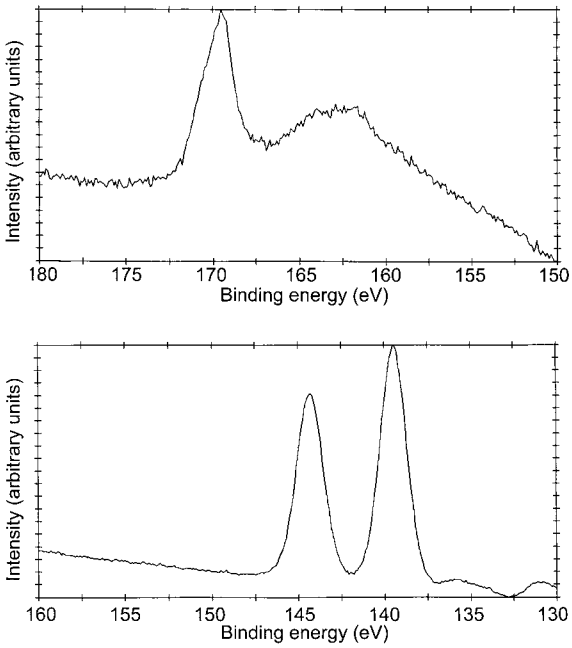

Figure 13. XPS spectrum of a product obtained at neutral pH. (a) The S(2p), and (b) the Pb(4f) regions of the spectrum are shown.

sulfide ions exist in the reaction product but that their environment is different from that in pure PbS. The differences observed may of course arise from the very small size of the PbS particles comprising the aggregates. The Pb(4f) signal with $4f_{7/2}$ and $4f_{5/2}$ peaks at 138.9 and 143.7 eV is displaced to higher energies with respect to that of a reference PbS sample (peaks at 137.5 and 142.4 eV). In addition, the widths of the two peaks are visibly smaller. The situation is strongly reminiscent of the results of Guo et al.[34] obtained with lead alkanoates before reaction with H_2S and formation of PbS particles. This Pb signal implies that "surface" lead is coordinated by oxygen,[35] although it is not clear what the source of oxygen is (it could be sulfate or acetate).

The XRD patterns of Figure 2 provide evidence for the existence of a layered structure at long times. Such XRD patterns are always obtained for ordered surfactant crystals and have, for example, been reported for crystalline films of ammonium surfactants,[36] for lead stearate films, deposited on glass substrates with the Langmuir−Blodgett method, after reaction with H_2S gas,[37] and for lead alkanoate and thioalkanoate films before reaction with H_2S.[38] For alkyl sulfate surfactants in particular, similar examples are provided in the work of Hirata and Iimura on complexes of sulfate surfactants with phenols and naphthols[39] and, in the work of Tolbert et al., on the formation of composites between iron oxides and sulfate surfactants.[40] The observed spacing of the layered material in Figure 2 is 31 Å, which is identical to the spacing observed for pure lead dodecyl sulfate. This is not equal to the length of two all-trans dodecyl sulfate chains, which is roughly 40−42 Å. The surfactant chains are therefore either tilted or interdigitated. Identification of the exact chain conformation is difficult. The usually fruitful idea of using alkyl sulfate surfactants with different chain lengths (e.g., C_{10}, C_{14}, etc.)[40,41] cannot be applied here in a straightforward way, because the interaction of the surfactant with the polymer is strongly affected by the length of the surfactant tail, as is the solubility of the surfactant and of its lead salt. We have unsuccessfully experimented with sodium decyl and tetradecyl sulfates. The tetradecyl sulfate has a very small solubility at room temperature, whereas the cmc of the decyl sulfate is quite high (33 mmol/L),[21] necessitating the use of high surfactant concentration in solution, which has an unpredictable effect on the chemical equilibria in the reaction solution. The existing single-crystal information on various dodecyl sulfate compounds suggests that chain tilting rather than chain interpenetration is the reason for the shortened spacing in the powder XRD spectra.[42] There is a large number of equally spaced peaks in the XRD spectrum of Figure 2e, indicating that the lamellar structure is almost perfectly ordered to a very long range. The fact that the peak intensity does not drop exponentially and does not have a maximum intensity at $q = 0$ ($2\theta = 0$) implies that the scattering centers (here predominantly the lead cations) might not lie on a single plane in each lamellar sheet.[41]

How does such a well-ordered lamellar structure develop from a situation of aggregated PbS particles? Do the $Pb(DS)_2$ particles develop independently in the presence of excess Pb^{2+} ions, do they exist from the beginning inside the aggregates of Figure 3, do they arise from the kinetically controlled dissolution of the PbS aggregates initially formed, or are the layered structures built *on* the PbS aggregates with some secondary nucleation mechanism? We have found evidence that $Pb(DS)_2$ development in the intermediate pH range can occur in a variety of ways. The TEM picture in Figure 5 implies that $Pb(DS)_2$ rodlike particles are built *independently* by slow dissolution of the initially formed PbS aggregates. In the TEM picture of Figure 14a, however, we see that other possibilities exist. Here, the $Pb(DS)_2$ superstructure appears in the form of a wedge connecting PbS aggregates. In this situation, $Pb(DS)_2$ forms almost by breaking apart a PbS aggregate from inside and from outside. A close-up of such a fragment in Figure 14b shows more clearly how the organic structure builds around the PbS aggregate, while at the same time the original PbS crystallites disintegrate. On the basis of such evidence, we believe that PbS aggregates form first, either by normal solution aggregation or by surface aggregation on initial $Pb(DS)_2$ sheets, and then slowly dissolve. In certain cases, their dissolution is even more dramatic. We have observed the formation of interesting nanotube-like structures, with well-ordered layers of small PbS particles. The conditions for formation of such structures are currently under investigation.

III.4. Fundamental Role of the pH Value. The effect of the pH value is both profound and dramatic. We will present selected results obtained by varying the pH, with lead acetate as the lead source, using typical concentrations of $[Pb^{II}] = 3.7$ mmol/L, $[S^{-II}] = 3.7$ mmol/L, [SDS] = 7.5 mmol/L, and [PEO] = 1.8 g/L. Note that the ratio of concentrations of lead, sulfide, and dodecyl sulfate is 1:1:2, in accordance with the stoichiometries of the two expected major precipitates, PbS and $Pb(DS)_2$, although a slight excess of Pb^{II} over S^{-II} is preferable.

The sequence of structures observed at intermediate pH values (roughly $6.5 < pH < 10.5$) was presented in section III.1 and discussed in section III.3. At the higher pH values of this range, we observe considerably smaller cylindrical PbS aggregates, coexisting with spherical particles which eventually predominate at $pH > 11$. A TEM picture of the reaction products at pH = 11.7 is shown in Figure 15. Small PbS aggregates are always present, as seen in Figure 15 and clarified by XRD measurements; however, the solution is dominated by large polyhedral structures with characteristic size of 1 μm or larger. XRD does not reveal lamellar ordering in these structures, which appear from their XRD patterns and FTIR spectra to be quite complicated and to contain hydroxyl and probably acetate groups. The reaction products at high pH values are still under investigation.

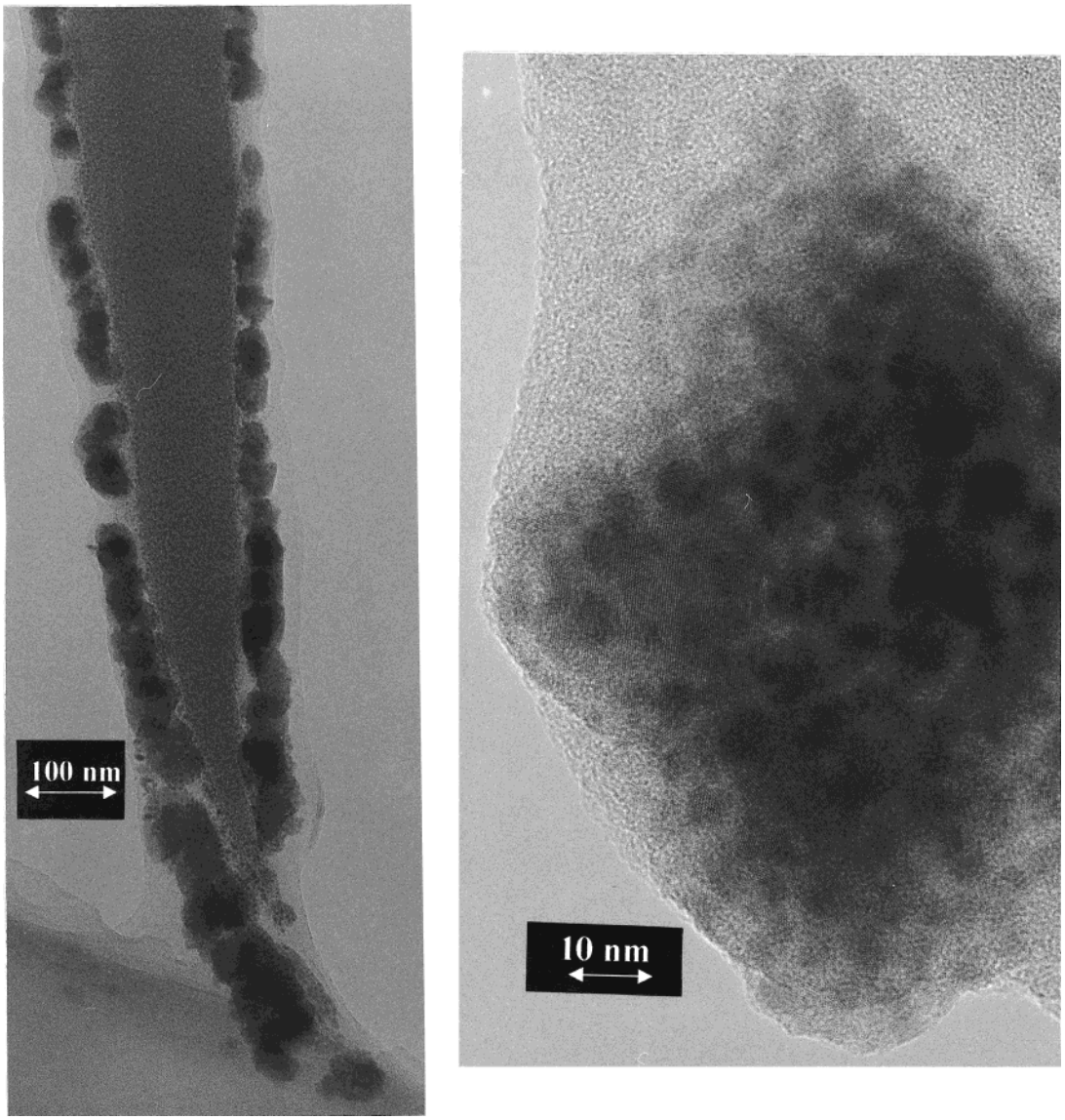

Figure 14. (a) TEM picture of $Pb(DS)_2$ structure developing from an original PbS aggregate. (b) High-resolution TEM detail showing a fragment of a PbS aggregate enveloped by $Pb(DS)_2$ growth.

TABLE 1: Behavior of the Crystallizing System as a Function of pH, with Lead Acetate and Lead Nitrate as Sources for Pb^{II} [a]

pH range	$Pb(CH_3COO)_2$ case	$Pb(NO_3)_2$ case
pH > 11.0	spherical particles − twinned crystals some PbS aggregates	
6.5 < pH < 10.0	rodlike PbS aggregates evolve into layered structures of $Pb(DS)_2$ through metastable structures. no $Pb(DS)_2$ is formed at high pH	PbS aggregates, smaller aspect ratios than those with $Pb(Ac)_2$
4.5 < pH < 6.5	$Pb(DS)_2$ sheets, occasional inclusions of PbS	mostly PbS, occasional sheetlike and needlelike $Pb(DS)_2$
pH < 4.0	mostly $Pb(DS)_2$	coexistence of $Pb(DS)_2$ with loose PbS aggregates

[a] The solution formulation used is $[Pb^{II}] = 3.7$ mmol/L, $[S^{-II}] = 3.7$ mmol/L, [SDS] = 7.5 mmol/L, and [PEO] = 1.8 g/L. pH ranges in the table are only approximate.

At lower pH values (roughly 4.0 < pH < 6.0), we observe a rapid crystallization of small PbS particles in the beginning, as well as some larger PbS particles (of sizes up to 1000 Å), around which the $Pb(DS)_2$ structure develops immediately, as evidenced by the XRD spectra presented in Figure 16. A striking TEM picture of such a system is shown in Figure 17, where we see large microbe-like organic structures containing PbS crystals as inclusions. Finally, for pH < 4.0, achieved with the addition of acetic acid, mostly $Pb(DS)_2$ is obtained, as evidenced by FTIR, ^{207}Pb NMR, HRTEM, and elemental analysis (results not shown). $Pb(DS)_2$ always appears in the form of thin, platelike crystallites in the low pH range (see TEM and polarizing microscopy pictures in the Supporting Information to this article) that can be easily identified with respect to PbS. Generally, low pH values favor the formation of pure $Pb(DS)_2$ when lead acetate is used as the lead source. The reason for this is the extremely low concentration of S^{2-} at low pH. We summarize the crystallization behavior of the system as a function of pH in Table 1.

III.5. Role of Surfactant Concentration, Polymer Concentration, and Solution Composition. If SDS is absent in the system, under otherwise similar concentrations of polymer,

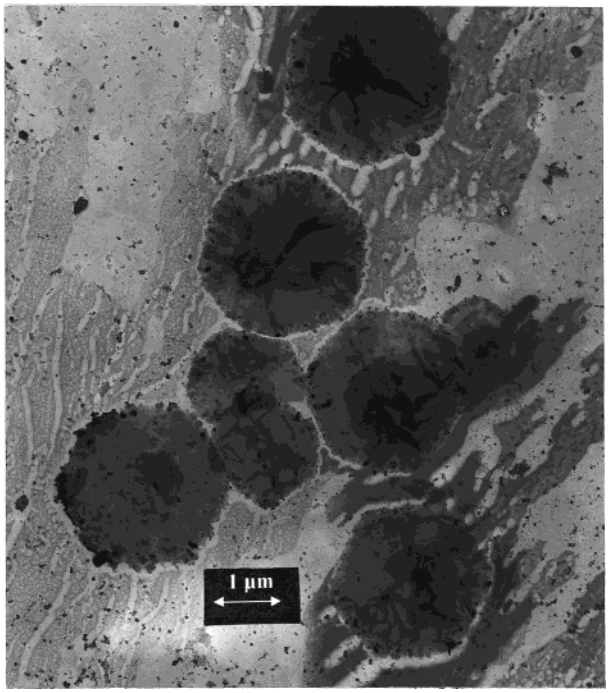

Figure 15. TEM picture of reaction products obtained at pH = 11.7. Some small PbS aggregates can be seen, but the dominant structures are large polyhedral particles with sizes up to and larger than 1 μm.

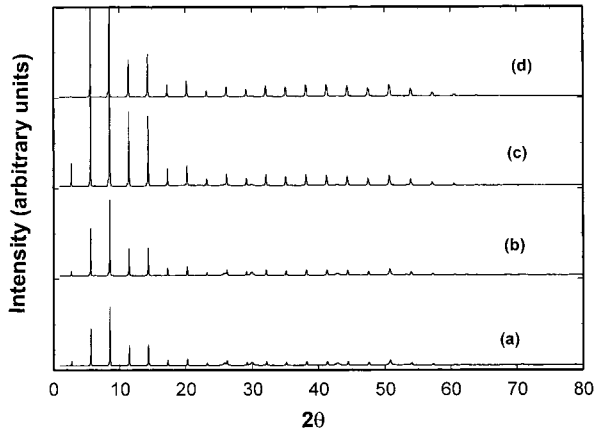

Figure 16. Time evolution of XRD patterns of crystallization products obtained with lead acetate at acidic pH. The patterns correspond to products obtained (a) 0, (b) 1, (c) 4, and (d) 10 days after reaction onset. The pH value was reduced to 4.5 by the addition of acetic acid.

Pb^{II}, and S^{-II}, small PbS particles are formed, as evidenced by XRD analysis and observed in previous work.[6] There is usually PbS precipitation in this case, unless very small concentrations of Pb^{2+} and S^{2-} are used, in which case the small particles are stabilized by the polymer chains and remain in suspension.

In the presence of SDS, but if no polymer is present, fewer small cylindrical aggregate structures are evident, similar to those visible in Figures 3 and 4, which do not grow with time as the particles in the presence of polymer do. We also observed randomly distributed PbS particles. The aggregated structures are not so well developed as those of Figure 3. These observations are compatible with the mechanism outlined in section III.2, according to which polymer chains are necessary for the rapid formation of aggregates of PbS crystallites.

The concentration and molecular weight of the polymer in the system play a significant role. One expects the bridging action of the polymer to be more efficient at higher concentrations or, at the same concentrations, for higher molecular weight.

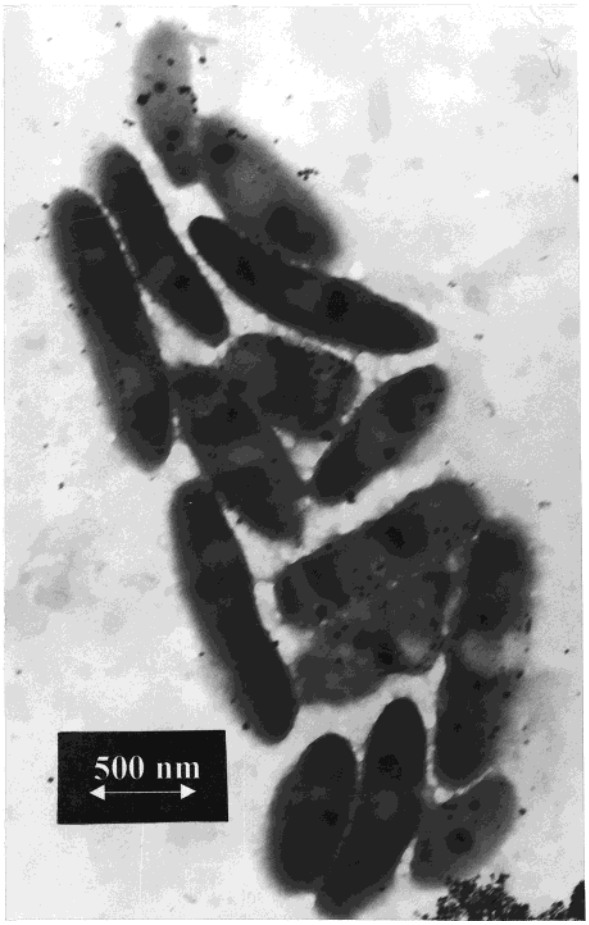

Figure 17. TEM picture of structures obtained at pH < 5 4 days after reaction onset. The organic structure develops surrounding small PbS particles that act as nucleating centers.

We have indeed observed that the number of composite aggregates of the type imaged in Figures 3 and 4 is significantly reduced at low PEO concentrations (<1 g/L for PEO of MW 2×10^5), when the polymer solution is truly dilute. One typically obtains a large number of loose PbS flocs (see TEM pictures in the Supporting Information). The opposite happens at higher polymer concentrations, when the solution is semidilute. For a semidilute solution of PEO with MW of 5×10^6, the development of the layered $Pb(DS)_2$ structure is fast, within a few days the system evolves to structures achieved only after considerably longer time with lower molecular weight polymer, as evidenced by XRD. Apparently, the bridging action of the polymer is enhanced, when chain-molecule interpenetration and entanglement sets in.

At constant Pb^{2+} and S^{2-} concentrations, the role of SDS concentration is easy to understand. Below the cac, no micelles are formed on the polymer chains and no rodlike PbS aggregates are observed by TEM. PbS crystallizes in solution in an ordinary way. Above the cmc, nucleation occurs on the polymer chains and on the free micelles in solution, and we obtain a more complex picture of aggregates and individual PbS crystallites (see the Supporting Information)

III.6. Importance of the Lead Source: Nitrate vs Acetate. When $Pb(NO_3)_2$ is used as the lead source the situation changes slightly, because much of the lead is now available in solution in the form of Pb^{2+} ions. This has the effect of considerably reducing the pH range over which $Pb(DS)_2$ can predominate or of forcing the coexistence of $Pb(DS)_2$ and PbS, even at quite low pH. At neutral and slightly basic pH, one still observes the

aggregation of primary PbS particles, but the aggregates are thicker: they do not have the characteristic rodlike morphology observed in the lead acetate case (see the Supporting Information). Table 1 also contains the behavior of the system as a function of pH for the $Pb(NO_3)_2$ case.

IV. Summary

In certain ways, the present system provides an opposite example compared to systems in which topotactic reactions form sulfide semiconductor particles in organized surfactant assemblies.[10−12,36−38] In the quoted systems, the organic structures preexist, with metal cations being organized in layers separated by the long organic chains. Introduction of H_2S gas leads to the formation of sulfide particles, preferentially on the original planes of the cations or on specifically targeted sites.[38] In the present system, the PbS particles are formed from the onset and aggregate in a surprisingly ordered fashion, eventually becoming scaffolds for the growth of layered organic structures.

The results presented in this paper illuminate an interesting example of the effect of competing chemical equilibria on inorganic crystallization in the complex environment of a polymer-surfactant solution. The crystallization of PbS is just an example from which one can draw conclusions of much wider significance. With regard to the crystallization process, the most important conclusions are as follows:

(a) If the surfactant interacts strongly with one of the ions of the inorganic salt, it may participate in the crystallization reaction and lead to completely different, and sometimes unexpected, products.

(b) The pH plays a fundamental role, if it regulates the concentration of reactive species. This is the case with S^{2-} and acetate ions in the present system. Decreasing the concentration of S^{2-} to very low levels leads to predomination of a reaction product, $Pb(DS)_2$, that is normally much more soluble than PbS.

(c) If the anions in the starting substances used as sources for the participating ions strongly coordinate to the metal centers, the structure of the reaction products can be different from that obtained in the alternative case. This is exemplified in the present work by the use of the nitrate and the acetate salts of lead. The nitrate salt releases a higher percentage of Pb^{2+} ions in solution and favors the production of PbS over a broader range of pH values, whereas the acetate salt releases a very small percentage of hydrated Pb^{2+} ions, facilitating the production of $Pb(DS)_2$. Similar effects can be anticipated if additional substances are present that interact with the reactive species. This is a very general conclusion and a well-known phenomenon in many crystallizing systems.[43]

The PbS aggregation process itself and the subsequent development of $Pb(DS)_2$ lamellar structures is not well understood. Formation of aggregates is an expected phenomenon in the presence of flocculating polymers. However, why should the aggregates adopt a cylindrical shape? What happens to the polymer once the aggregates are formed? Furthermore, how is the organic lattice built from the PbS aggregate? These difficult questions regarding the mechanisms of processes that may be either thermodynamically or kinetically controlled or both cannot be fully answered only on the basis of the experiments presented in this paper. It is important to note here that over broad ranges of pH and composition various products of the crystallization reaction coexist.

A second group of conclusions refers to the supramolecular system that is chosen in the present investigation as the crystallization medium:

(a) The role of polymer type is significant and multifaceted. Strong interaction with the surfactant molecules ensures that the subsequent nucleation and crystallization will be largely localized in the vicinity of polymer chains. In addition, if the polymer has very strong specific interactions with the cations, it can also influence the crystallization process in a profound way. Finally, the polymer determines the rate at which bridging flocculation of the primary crystals occurs.

(b) Polymer concentration is important. Apparently, chain interpenetration in semidilute solutions allows for a faster bridging flocculation process and a fast formation of the aggregates that eventually evolve into the layered structures observed in this work.

(c) Surfactant concentration must be carefully controlled between the cac and the cmc. If no association with the polymer occurs, the bridging mechanism of the polymer does not operate. On the other hand, if micelles exist in solution away from the polymer chains, we get PbS nucleation and crystallization in the bulk of the solution as well and the crystallization process may yield many different products.

Finally the cation/anion system is at the core of the crystallization process. Interactions of cations and anions with the polymer chains and the surfactant molecules can lead to a tremendous variety of crystallization phenomena. We will present a limited number of examples in the future, to prove that polymer/surfactant solutions provide a rich and until now largely unexplored terrain for inorganic chemistry and materials synthesis.

Acknowledgment. We would like to thank Dr. Daniel Schneider (Department of Materials, ETH) for assistance with the XRD measurements. E.L. and T.K.-L. thank Maria Orfanou (Department of Chemistry, Cyprus) for general laboratory help. This work was partly supported by funds from ETH and the University of Cyprus.

Supporting Information Available: Figures S1−S5 showing TEM images. This material is available free of charge via the Internet at http://pubs.acs.org.

References and Notes

(1) Ozin, G. A. *Adv. Mater.* **1992**, *4*, 612. Chan, Y. N. C.; Craig, G. S. W.; Schrock, R. R.; Cohen, R. E. *Chem. Mater.* **1992**, *4*, 885. Heywood, B. R.; Mann, S. *Adv. Mater.* **1994**, *6*, 9. Fendler, J. H.; Meldrum, F. C. *Adv. Mater.* **1995**, *7*, 607. Braun, P. V.; Osenar, P.; Stupp, S. I. *Nature* **1996**, *380*, 325. Göltner, C. G.; Antonietti, M. *Adv. Mater.* **1997**, *9*, 431. Antonietti, M.; Göltner, C. *Angew. Chem., Int. Ed. Engl.* **1997**, *36*, 910. Antonietti, M.; Gröhn, F.; Hartmann, J.; Bronstein, L. *Adv. Mater.* **1997**, *36*, 2080. Selvan, S. T.; Spatz, J. P.; Klok, H.-A.; Möller, M. *Adv. Mater.* **1998**, 10, 132. Bronstein, L. M.; Platonova, O. A.; Yakunin, A. N.; Yanovskaya, I. M.; Valetzky, P. M.; Dembo, A. T.; Makhaeva, E. E.; Mironov, A. V.; Khokhlov, A. R. *Langmuir* **1998**, *14*, 252. Ying, J. Y.; Mehnert, C. P.; Wong, M. S. *Angew. Chem., Int. Ed. Engl.* **1999**, *38*, 56. Lu, Y.; Cao, G.; Kale, R. P.; Prabakar, S.; López, G. P.; Brinker, C. J. *Chem. Mater.* **1999**, *11*, 1223. Zhao, M.; Crooks, R. M. *Adv. Mater.* **1999**, *11*, 217. Spatz, J. P.; Herzog, T.; Mößmer, T.; Ziemann, P.; Möller, M. *Adv. Mater.* **1999**, *11*, 149.

(2) Kommareddi, N. S.; Tata, M.; John, V. T.; McPherson, G. L.; Herman, M. F.; Lee, Y.-S.; O'Connor, C. J.; Akkara, J. A.; Kaplan, D. L. *Chem. Mater.* **1996**, *8*, 801. Breulmann, M.; Cölfen, H.; Hentze, H.-P.; Antonietti, M.; Walsh, D.; Mann, S. *Adv. Mater.* **1998**, *10*, 237. Duxin, N.; Brun, N.; Colliex, C.; Pileni, M. P. *Langmuir* **1998**, *14*, 1984.

(3) Fogg, D. E.; Radzilowski, L. H.; Dabbousi, B. O.; Schrock, R. R.; Thomas, E. L.; Bawendi, M. G. *Macromolecules* **1997**, *30*, 8433.

(4) Wang, Y.; Herron, N. *Science* **1996**, *273*, 632. Beecroft, L. L.; Ober, C. K. *Chem. Mater.* **1997**, *9*, 1302. Sooklal, K.; Hanus, L. H.; Ploehn, H. J.; Murphy, C. J. *Adv. Mater.* **1998**, *10*(*14*), 1083. Sanchez, C.; Ribot, F.; Lebeau, B. *J. Mater. Chem.* **1999**, *9*, 35.

(5) Antonelli, D. M.; Ying, J. Y. *Chem. Mater.* **1996**, *8*, 874. Klingelhöfer, S.; Heitz, W.; Greiner, A.; Oestreich, S.; Förster, S.; Antonietti, M. *J. Am. Chem. Soc.* **1997**, 119, 10116. Seregina, M. V.; Bronstein, L.

M.; Platonova, O. A.; Chernyshov, D. M.; Valetsky, P. M.; Hartmann, J.; Wenz, E.; Antonietti, M. *Chem. Mater.* **1997**, *9*, 923.

(6) Kyprianidou-Leodidou, T.; Caseri, W.; Suter, U. W. *J. Phys. Chem.* **1994**, *98*, 8992.

(7) Lianos, P.; Thomas, J. K. *J. Colloid Interface Sci.* **1987**, *117*, 505. Ward, A. J. I.; O'Sullivan, E. C.; Rang, J.-C.; Nedljkovic, J.; Patel, R. C. *J. Colloid Interface Sci.* **1993**, *161*, 316. Ogawa, S.; Hu, K.; Fan, F.-R. F.; Bard, A. J. *J. Phys. Chem. B* **1997**, *101*, 5707.

(8) Yang, J. P.; Qadri, S. B.; Ratna, B. R. *J. Phys. Chem.* **1996**, *100*, 17255.

(9) Zhao, X. K.; Yang, J.; McCormick, L. D.; Fendler, J. H. *J. Phys. Chem.* **1992**, *96*, 9933. Yang, J.; Fendler, J. H. *J. Phys. Chem.* **1995**, *99*, 5505.

(10) Li, L. S.; Qu, L.; Wang, L.; Lu, R.; Peng, X.; Zhao, Y.; Li, T. J. *Langmuir* **1997**, *13*, 6183.

(11) Guo, S.; Popovitz-Biro, R.; Arad, T.; Hodes, G.; Leiserowitz, L.; Lahav, M. *Adv. Mater.* **1998**, *10*, 657.

(12) Kane, R. S.; Cohen, R. E.; Silbey, R. *Chem. Mater.* **1996**, *8*, 1919. Schneider, T.; Haase, M.; Kornowski, A.; Naused, S.; Weller, H.; Förster, S.; Antonietti, M. *Ber. Bunsen.-Ges. Phys. Chem.* **1997**, *101*, 1654. Zeng, Z.; Wang, S.; Yang, S. *Chem. Mater.* **1999**, *11*, 3365. Dutta, A. K.; Ho, T.; Zhang, L.; Stroeve, P. *Chem. Mater.* **2000**, *12*, 1042. Pitcher, M. W.; Cates, E.; Raboin, L.; Bianconi, P. A. *Chem. Mater.* **2000**, *12*, 1738.

(13) Nozik, A. J.; Williams, F.; Nenadović, M. T.; Rajh, T.; Mićić, O. I. *J. Phys. Chem.* **1985**, *89*, 397. Rossetti, R.; Hull, R.; Gibson, J. M.; Brus, L. E. *J. Chem. Phys.* **1985**, *83*, 1406. Gallardo, S.; Gutiérrez, M.; Henglein, A.; Janata, E. *Ber. Bunsen-Ges. Phys. Chem.* **1989**, *93*, 1080.

(14) Wang, S.; Yang, S. *Langmuir* **2000**, *16*, 389.

(15) Leontidis, E.; Kyprianidou-Leodidou, T.; Caseri, W.; Kyriakou, K. *Langmuir* **1999**, *15*, 3381.

(16) Goddard, E. D. *Colloids Surf.* **1986**, *19*, 255. Brackman, J. C.; Egberts, J. B. F. N. *Chem. Soc. Rev.* **1993**, *85*. Jönsson, B.; Lindman, B.; Holmberg, K.; Kronberg, B. *Surfactants and Polymers in Aqueous Solution*; Wiley: New York, 1998.

(17) Cabane, B. *J. Phys. Chem.* **1977**, *81*, 1639. Cabane, B.; Duplessix, R. *J. Phys. (Paris)* **1982**, *43*, 1529. Cabane, B.; Duplessix, R. *J. Phys. (Paris)* **1987**, *48*, 651. Jones, M. N. *J. Colloid Interface Sci.* **1967**, *23*, 36. Schwuger, M. J. *J. Colloid Interface Sci.* **1973**, *43*, 491. Gao, Z.; Wasylishen, R. E.; Kwak, J. C. T. *J. Phys. Chem.* **1991**, *95*, 462. Xia, J.; Dubin, P. L.; Kim, Y. *J. Phys. Chem.* **1992**, *96*, 6805. Van Stam, J.; Almgren, M.; Lindblad, C. *Prog. Colloid Pol. Sci.* **1991**, *84*, 13. D'Aprano, A.; La Mesa, C.; Persi, L. *Langmuir* **1997**, *13*, 5876. Fox, G. J.; Bloor, D. M.; Holzwarth, J. F.; Wyn-Jones, E. *Langmuir* **1998**, *14*, 1026.

(18) Stoll, S.; Buffle, J. *J. Colloid Interface Sci.* **1996**, 180, 548.

(19) The critical concentration for chain interpenetration in a polymer solution is given by

$$C^* = \frac{\bar{M}_n}{(4\pi/3)R_g^3}$$

where $\bar{M}_n$ is the average molecular weight and R_g is the radius of gyration. For the PEO of MW 2×10^5, we have found from viscosity measurements that the radius of gyration is 200 ± 20 Å; hence, C^* is in the range of 10 ± 3 g/L. Because $R_g \approx \bar{M}_n^{0.6}$ for polymers in good solvents, the critical concentration C^* for polymers with molecular weights 5×10^6 is below 1 g/L.

(20) Bennet, A. E.; Rienstra, C. M.; Auger, M.; Lakshmi, K. V.; Griffin, R. G. *J. Chem. Phys.* **1995**, *103*, 6951.

(21) Evans, D. F.; Wennerström, H. *The Colloidal Domain*, 2nd ed.; Wiley-VCH: New York, 1999.

(22) Scherrer, P. *Nachr. Königl. Ges. Wiss. Göttingen, Math.-Phys. Klasse* **1918**, 98. Taylor, A. *X-ray Metallography*; Wiley & Sons: New York, 1961.

(23) *CRC Handbook of Chemistry and Physics*, 65th ed.; CRC Press: Boca Ratton, FL, 1984.

(24) Day, R. A.; Underwood, J. R. *Quantitative Analysis*, 5th ed.; Prentice Hall: New York, 1986.

(25) Sreenivasarao, K.; Doyle, F. M. *Separ. Pur. Technol.* **1997**, *12*, 157.

(26) Leontidis, E. et al. Unpublished results.

(27) Nancollas, G. H. *J. Chem. Soc.* **1955**, 1458. Altounian, N.; Glatfelter, A.; Bai, S.; Dybowski, C. *J. Phys. Chem. B* **2000**, *104*, 4723.

(28) Stumm, W.; Morgan, J. J. *Aquatic Chemistry*; Wiley-Interscience: New York, 1996.

(29) Harrison, P. G.; Healy, M. A.; Steel, A. T. *J. Chem. Soc., Dalton Trans.* **1983**, 1845.

(30) Hummel, D. O.; Scholl, F. *Atlas of Polymer and Plastics Analysis*, 2nd ed.; Carl Hanser Verlag: München, Germany, 1984.

(31) Kartha, V. B.; Leitch, L. C.; Mantsch, H. H. *Can. J. Chem.* **1984**, *62*, 128. Tomačić, V.; Popović, S.; Tuček-Boćić, Lj.; Pucić, I.; Filipović-Vinceković, N. *Ber. Bunsen-Ges. Phys. Chem.* **1997**, *101*, 1942. Sperline, R. P. *Langmuir* **1997**, *13*, 3715. Sperline, R. P.; Song, Y.; Freiser, H. *Langmuir* **1997**, *13*, 3727.

(32) Sperline, R. P.; Song, Y.; Freiser, H. *Langmuir* **1992**, *8*, 2183. Couzis, A.; Gulari, E. *Langmuir* **1993**, *9*, 3414. Suga, K.; Rusling, J. F. *Langmuir* **1993**, 9, 3649.

(33) Feio, G.; Burrows, H. D.; Geraldes, C. F. G. C.; Pinheiro, T. J. T. *Liq. Cryst.* **1991**, *9*, 417. Neue, G.; Dybowski, C.; Smith, M. L.; Hepp, M. A.; Perry, D. L. *Solid State Nucl. Magn. Res.* **1996**, *6*, 241. Zhao, P.; Prasad, S.; Huang, J.; Fitzgerald, J. J.; Shore, J. S. *J. Phys. Chem. B* **1999**, *103*, 10617. Teff, D. J.; Caulton, K. G. *Inorg. Chem.* **1999**, *38*, 2240.

(34) Guo, S.; Popovitz-Biro, R.; Weissbuch, I.; Cohen, H.; Hodes, G.; Lahav, M. *Adv. Mater.* **1998**, *10*, 121.

(35) Muilenberg, G. E., Ed.; *Handbook of X-ray Photoelectron Spectroscopy*; Perkin-Elmer Corporation: Eden Prairie, MN, 1978.

(36) Ishikawa, Y.; Kunitake, T. *J. Am. Chem. Soc.* **1991**, *113*, 621. Ichinose, I.; Kimizuka, N.; Kunitake, T. *J. Phys. Chem.* **1995**, *99*, 3736.

(37) Peng, X.; Chen, H.; Kan, S.; Bai, Y.; Li, T. *Thin Solid Films* **1994**, *242*, 118. Ganguly, P.; Sastry, M.; Choudhury, S.; Paranjape, D. V. *Langmuir* **1997**, *13*, 6582.

(38) Guo, S.; Popovitz-Biro, R.; Arad, T.; Hodes, G.; Leiserowitz, L.; Lahav, M. *Adv. Mater.* **1998**, *10*, 657. Guo, S.; Konopny, L.; Popovitz-Biro, R.; Cohen, H.; Porteanu, H.; Lifshitz, E.; Lahav, M. *J. Am. Chem. Soc.* **1999**, *121*, 9589.

(39) Hirata, H.; Iimura, N. *J. Colloid Interface Sci.* **1998**, *199*, 111.

(40) Tolbert, S. H.; Sieger, P.; Stucky, G. D.; Aubin, S. M. J.; Wu, C.-C.; Hendrickson, D. N. *J. Am. Chem. Soc.* **1997**, *119*, 8652.

(41) Arkas, M.; Yannakopoulou, K.; Paleos, C. M.; Weber, P.; Skoulios, A. *Liq. Cryst.* **1995**, *18*(*4*), 563.

(42) Sundell, S. *Acta Chem. Scand.* **1977**, *A31*, 799. Coiro, V. M.; Mazza, F.; Pochetti, G. *Acta Crystallogr.* **1986**, *C42*, 991. Coiro, V. M.; Manigrasso, M.; Mazza, F.; Pochetti, G. *Acta Crystallogr.* **1987**, *C43*, 850. Coiro, V. M.; Mazza, F. *Acta Crystallogr.* **1989**, *C45*, 1132.

(43) McFadyen, P.; Matijeviæ, E. *J. Colloid Interface Sci.* **1973**, *44*, 95. Chiu, G.; Meehan, E. J. *J. Colloid Interface Sci.* **1974**, *49*, 160. Sugimoto, T. *Adv. Colloid Int. Sci.* **1987**, *28*, 65. Sugimoto, T.; Chen, S.; Muramatsu, A. *Colloids Surf. A* **1998**, *135*, 207. Doxsee, K. M. *Chem. Mater.* **1998**, *10*, 2610.